



**HAL**  
open science

## Heterogeneous tensile behavior of impact-modified polypropylene plates processed by injection moulding

Olivier de Almeida, Fabienne Touchard, Laurence Chocinski-Arnault

► **To cite this version:**

Olivier de Almeida, Fabienne Touchard, Laurence Chocinski-Arnault. Heterogeneous tensile behavior of impact-modified polypropylene plates processed by injection moulding. PPS 26 -The Polymer Processing Society 26th Annual meeting, Jul 2010, Banff, Canada. 11 p. hal-01760276

**HAL Id: hal-01760276**

**<https://hal.science/hal-01760276>**

Submitted on 4 Nov 2020

**HAL** is a multi-disciplinary open access archive for the deposit and dissemination of scientific research documents, whether they are published or not. The documents may come from teaching and research institutions in France or abroad, or from public or private research centers.

L'archive ouverte pluridisciplinaire **HAL**, est destinée au dépôt et à la diffusion de documents scientifiques de niveau recherche, publiés ou non, émanant des établissements d'enseignement et de recherche français ou étrangers, des laboratoires publics ou privés.

# HETEROGENEOUS TENSILE BEHAVIOR OF IMPACT-MODIFIED POLYPROPYLENE PLATES PROCESSED BY INJECTION MOULDING

O. De Almeida<sup>1,2</sup>, F. Touchard<sup>3</sup>, L. Chocinski-Arnault<sup>3</sup>

1- Université de Toulouse ; INSA, UPS, Mines Albi, ISAE ; ICA (Institut Clément Ader); Campus Jarlard, F-81013 Albi cedex 09, France

2- Ecole des Mines Albi, Campus Jarlard, F-81013 Albi, France – olivier.dealmeida@mines-albi.fr

3 – Institut P<sup>3</sup>, UPR 3346, Département Physique et Mécanique des Matériaux ; ENSMA, 1, avenue Clément Ader, 86961 Futuroscope Chasseneuil – fabienne.touchard@lmpm.ensma.fr; laurence.chocinski@lmpm.ensma.fr

**Abstract** – Due to the fast cooling of polymer on the mould surface, the injection moulding process is known to be responsible of property gradients through thickness. Nevertheless, the mechanical behaviour is usually characterized by considering an homogeneous polymer, even when tensile test specimens processed by injection moulding are used. In order to characterize the local three-dimensional behaviour, a new set up based on digital image correlation has been developed and applied to specimens machined from injection moulded plates. This experimental set up allows to measure the strain fields on both front and lateral sides of specimens with a good accuracy. In this study, two impact modified polypropylenes have been analyzed under tensile loading. These polymers are made of ethylene-propylene rubber nodules and lamellar talc particles embedded in a polypropylene matrix. They differ from the volumetric amount of talc (4% in material A, 0,5% in material B). Unlike neat polypropylene, these materials do not exhibit a necking phenomenon in tension. The axial strain and transverse strain through specimen width remain homogeneous along the gauge length during the tensile test. On the other hand, the transverse strains through thickness differ for both polymers. Polymer B exhibits large gradients of  $\epsilon_{zz}$  strain between the centre and the plate surfaces while polymer A presents an homogeneous transverse deformation. As confirmed by microstructure investigation, these results reveal a large volumetric dilatation due to void growth for both polymers, but for polymer B, the large transverse gradient measured is due to a high volumetric dilatation gradient through plate thickness. The good thermal conductivity of talc could explain the different behaviour between the two polymers and the origin of volumetric dilatation gradient. In polymer B, the different cooling rates between plate core and surfaces induce large residual stresses which could create damage and initiate voids in plate core.

## Introduction

Injection moulding is one of the most widely used plastic part processing and the mechanical properties of thermoplastics are usually identified on moulded samples in considering that the material is homogeneous within the entire gauge volume.

Many studies have though revealed the existence of a skin/core structure in injection moulding process (Viana, 2004). In particular, Pennington et al (1999) and Stegge and Urban (2001) have shown that the skin structure of impact-modified polypropylenes is characterized by a stratification composed of different microstructure layers under the surface of injected plates.

The aim of this study has been to analyse the mechanical behaviour and the deformation mechanisms upon tensile loading of two impact-modified polypropylenes processed by injection moulding.

In order to characterize the deformation mechanisms upon stretching, the strain fields on the surface of the specimens have been measured by digital image correlation. In that way, an experimental set-up has

been developed and has allowed to measure strains with a good accuracy on the front and lateral surfaces of the specimens.

## Experimental

### Materials

The materials investigated in this study are two commercial impact-modified polypropylenes, used for automotive applications as car-bumpers. They were manufactured by Sabic under the references PP Compound 7510 (A) and 108MF97 (B) and provided in granule form. Composite A is a blend of polypropylene, ethylene-propylene-diene terpolymer (EPDM) and talc particles, while composite B is a copolymer of polypropylene and ethylene-propylene rubber (EPR) blended with talc.

The elastomeric and polypropylene phases are immiscible which induces a similar microstructure for both materials A and B. It is characterized by micrometric talc and elastomeric particles (0,5 $\mu$ m diameter) embedded in a polypropylene matrix.

Thermogravimetric analysis (TGA) and weight measurements have been performed on materials A

and B in order to quantify the phase weight proportions and the materials density (Delaval et al., 2009). The results are summarized in Tab. 1. They show that the main difference between these materials is the talc content : composite A contains 10%wt of talc, whereas composite B contains only 0,5%wt. It corresponds for polymers A and B to a volumetric ratio of 4% and 0,5% respectively, in considering a talc density of  $2,7\text{g}\cdot\text{cm}^{-3}$ .

		A	B
Density ( $\text{g}\cdot\text{cm}^{-3}$ )		0,955	0,895
Weight ratio	Polypropylene	0,695	0,775
	Elastomer	0,200	0,220
	Talc	0,105	0,005

**Tab. 1** – Composition of impact-modified polypropylenes

As confirmed by differential scanning calorimetry (DSC), the organic phases of the materials have similar physical properties. In polymers A and B, the polypropylene melting temperature is  $167^\circ\text{C}$  and the degree of crystallinity is about 49-50%wt. Moreover, in both materials, a crystalline structure has also been identified whose melting temperature has been recorded by DSC between  $113$  and  $115^\circ\text{C}$ . This melting temperature corresponds to polyethylene polymerized during the elastomer synthesis.

#### Sample preparation

Both polymers were injection moulded into  $300\times 100\times 3\text{mm}^3$  plates at the LRMP of St Etienne<sup>1</sup> and tensile specimens with gauge volume dimensions of  $10\times 10\times 3\text{mm}^3$  were machined from the moulded plates. A minimum distance of 20mm between the specimen gauge volume and the plate edges has been respected for all the specimens.

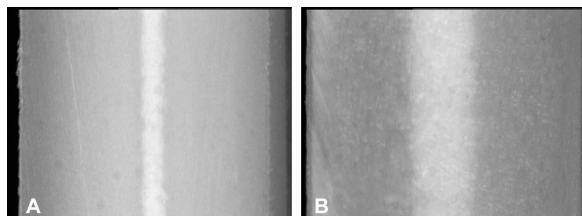


**Fig. 1** – Side view of the machined samples observed by optical microscopy (thickness = 3mm)

As observed by optical microscopy after machining, the polymer plates exhibit a different aspect between the core and the surface of the plates (Fig. 1). This optical heterogeneity supposes a different microstructure through plates thickness and is

<sup>1</sup> Laboratoire de Rhéologie des Matières Plastiques, CNRS, UMR 5156 - 23, rue du Docteur Paul Michelon

observable in both polymers. Nevertheless, these heterogeneities could not be confirmed by SEM investigation.

#### Experimental set-up

Deformation mechanisms of the impact-modified polypropylene have been studied upon stretching and characterized by digital image correlation. Tensile tests have been performed with an electromechanical test machine Instron 4505, at room temperature and with a constant cross head speed of  $10\text{mm}\cdot\text{min}^{-1}$ .

The front and lateral sides of the tensile specimens have been previously covered with a random speckle pattern whose average white and black grain diameter is  $30\mu\text{m} \pm 5\mu\text{m}$  (Brillaud et Lagattu-Touchard, 2002). Due to the grain fineness, a special experimental set-up has been developed so as to take the pictures of the speckle patterns during the tensile tests. It is composed of a mechanical device supporting a digital camera and a mirror (Fig. 2). This device allows to position the camera close to the specimen and in front of a constant centred volume. The mirror is also fastened on the device in such a way to reflect the lateral pattern of the specimen to the camera sensor.

In this configuration, the CCD matrix of  $2272\times 1704$  pixels<sup>2</sup> is separated from the specimen by about 10cm. Thus, an area of  $18\times 24$  mm<sup>2</sup> is in shot of the digital camera and one pattern grain is defined by about  $3\times 3$  pixels<sup>2</sup> on the CCD matrix.

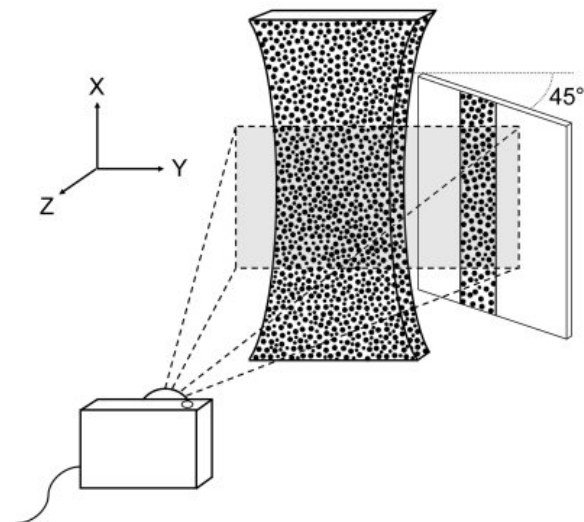


**Fig. 2** - Schematic representation of the experimental set-up.

By using this set-up, pictures of the front and the lateral patterns have been taken regularly during the tensile tests. The use of a camera has required short stops

- 42023 St Etienne Cedex 02 - France. Tel: 0477481554 - Fax: 0477485126

during the tests to record the images of front and lateral patterns. Nevertheless, it has been confirmed that the stops did not have influence on the tensile behaviour of the polymers. For further information about the testing procedure, the reader can refer to De Almeida et al. (2008).

#### Digital images exploitation

The digital image correlation (DIC) of the speckle patterns has been performed with a home developed software Granu. This software is based on the direct correlation of the discrete matrix of the pixel grey levels of a subwindow (Brillaud and Lagattu-Touchard, 2002). The displacement of each subwindow is ascribed to the centre point of the subwindow and the spatial resolution is defined as the real size of the subwindows.

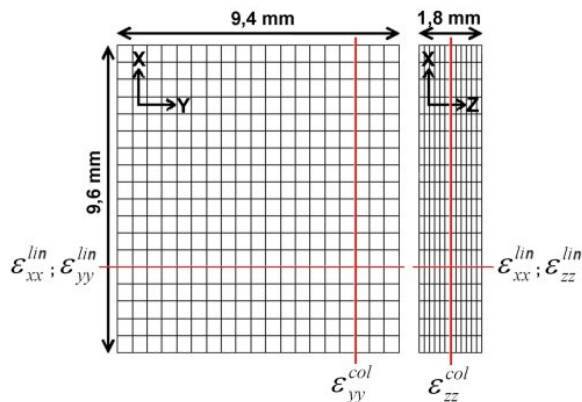


**Fig. 3** – Dimensions of sample zones within digital image correlation has been performed to measure displacements (each mesh node corresponds to a measurement point on the sample surface).

For all experiments, the in-plane displacement fields are incrementally obtained, starting with the undeformed image, by correlating subwindows of the speckle pattern from one image to the next with an adaptive mesh. The configuration chosen in this study allows in-plane displacement measurements with good accuracy, on both front and lateral sides of the specimens. With a magnification of 11.5  $\mu\text{m}/\text{pixel}$  for front images and 11.1  $\mu\text{m}/\text{pixel}$  for lateral images, the local displacements have been measured with respectively a spatial resolution, i.e. a correlation subwindow area, of 460 $\times$ 460  $\mu\text{m}^2$  and 440 $\times$ 440  $\mu\text{m}^2$ . Digital image correlation has been performed in about 400 measurement points on the front side and about 250 on the lateral side on areas corresponding respectively to 9.4 $\times$ 9.6 mm<sup>2</sup> (Width $\times$ Length) and 1.8 $\times$ 9.6 mm<sup>2</sup> (Thickness $\times$ Length) (Fig. 3). The Granu software processing time is about five seconds for 400 measurement points with a current personal computer.

The Abaqus software has then been used to derive experimental data using large-strain formalisms (Hencky strain), and using a small-strain formalism, afterwards called nominal strain (Cauchy strain). This can be performed with an Abaqus file within the subwindow centre points are written as nodes of a mesh and displacements are treated as boundary conditions. Local true axial strains  $\epsilon_{xx}$  are thus calculated from both front and lateral vertical displacements (x-axis), while local front transverse strains  $\epsilon_{yy}$  (y-axis) and local lateral transverse strains  $\epsilon_{zz}$  (z-axis) are respectively determined from horizontal front and lateral displacements.

Because of the mesh regularity, the average of the local axial strain  $\epsilon_{xx}^{av}$  and of the transverse strains  $\epsilon_{yy}^{av}$  and  $\epsilon_{zz}^{av}$  can be calculated from the results of digital image correlation.  $\epsilon_{xx}^{av}$  has been used to characterize the tensile test progress i.e. the global strain applied to the specimen.

The average strains  $\epsilon_{xx}^{lin}$ ,  $\epsilon_{yy}^{lin}$ ,  $\epsilon_{zz}^{lin}$ ,  $\epsilon_{yy}^{col}$ ,  $\epsilon_{zz}^{col}$  have also been calculated from the local strain measurements. As shown in Fig. 3, they correspond to the average of the local strains per line (lin) or per column (col) in all three dimensions.

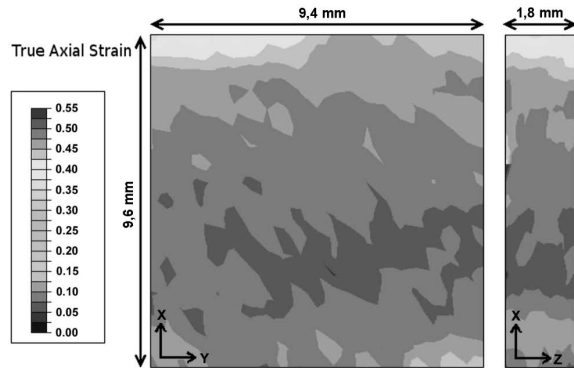
## Results and Discussion

### Homogeneous axial deformation

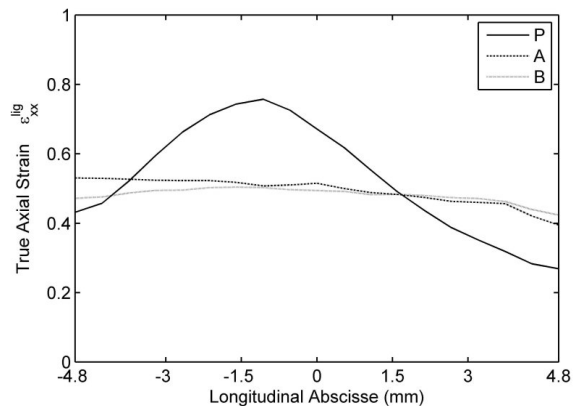
For both materials, the measurements have been performed regularly during the tensile tests until grain pattern degradation. The last step, for which digital image correlation was possible and for which the results were conclusive, corresponds to an average axial strain  $\epsilon_{xx}^{av}$  of 49% for both polymers. The axial strain fields of front and lateral surfaces for  $\epsilon_{xx}^{av} = 49\%$  are presented in Fig. 4 for polymer B. A good agreement can be noticed between the strain fields measured on both surfaces and this has been observed for each measurement step.

Fig. 5 shows the comparison of the average axial strain per line  $\epsilon_{xx}^{lin}$  measured for a neat polypropylene and for the two impact-modified polypropylenes. The necking phenomenon observed in polypropylene is characterized by a large axial gradient. The axial strain reaches about 80% in the neck while it is only 27% close to the analysed surface. On the other hand, for both impact-modified polypropylenes, the axial strain is ranged between 45 and 55% along the specimen for an average axial strain  $\epsilon_{xx}^{av}$  of 49%. The deformation of this materials upon stretching can thus be considered as homogeneous along the gauge length,

and the average strains  $\epsilon_{yy}^{col}$  and  $\epsilon_{zz}^{col}$  can be used to analyse the deformation behaviour of polymers A and B through specimen width and thickness. This homogeneous axial deformation is induced by the elastomer phase which has already been noticed in high-impact PS by G'sell et al. (2002).



**Fig. 4** – Axial strain fields of polymer B measured on front and lateral sides of the specimen for an average axial strain  $\epsilon_{xx}^{av}$  of 49%.



**Fig. 5** – Axial strain profile along the strain gauge for polymers A and B. Comparison with the strain profile measured for a neat polypropylene P.

#### Transverse strains

The transverse strain fields of material B for  $\epsilon_{xx}^{av} = 49\%$  are shown in Fig. 6 and the transverse strain profiles through specimen width (W) and thickness (T) are presented in Fig. 7 and Fig. 8. As the deformation of the impact-modified polypropylenes are axially homogeneous, the profiles are plotted with the average transverse strain per column  $\epsilon_{yy}^{col}$  and  $\epsilon_{zz}^{col}$ . On one hand, these average strains are representative of the whole specimen length and on the other hand, they provide a smoother strain profile.

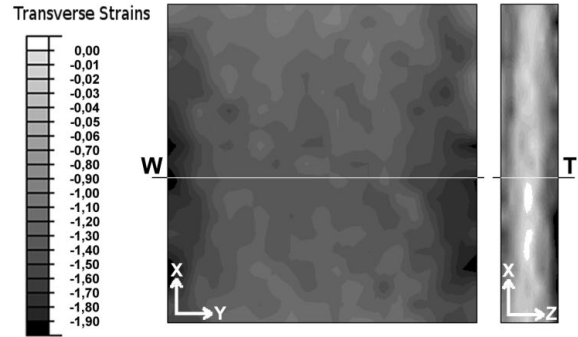


**Fig. 6** – Transverse strains fields of polymer B measured on front and lateral sides of the specimen for an average axial strain of 49%.

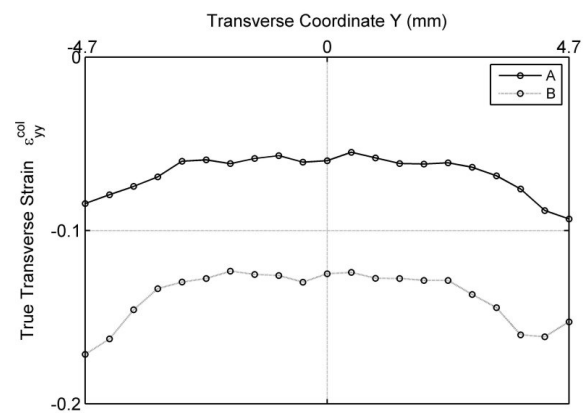


**Fig. 7** – Transverse strain profiles measured in polymers A and B through specimen thickness ( $\epsilon_{zz}^{col}$ ) for  $\epsilon_{xx}^{av} = 49\%$ .

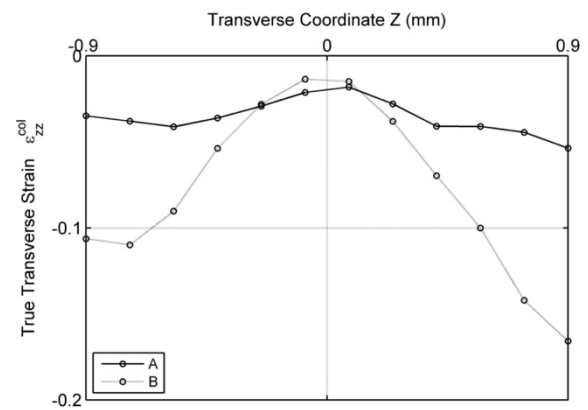


**Fig. 8** – Transverse strain profiles measured in polymers A and B through specimen width ( $\epsilon_{yy}^{col}$ ) for  $\epsilon_{xx}^{av} = 49\%$ .

As shown in Fig. 7, the transverse strain through specimen width is around -0.15 in material B when it

is only  $-0.07$  in material A for an axial strain of 49%. The width reduction of the specimen is then larger in polymer B than in polymer A. Moreover, the strain profiles are not constant through specimen width. On both sides of the centre 6mm of the specimen gauge, the transverse strain decreases.

Through specimen thickness, shown in Fig. 8, the two impact-modified polypropylenes exhibit different strain profiles. In specimen core, the transverse strain  $\epsilon_{zz}^{col}$  is almost nil (around  $-0.01$ ) for polymers A and B. But whereas polymer A exhibits a constant transverse strain  $\epsilon_{zz}^{col}$  through specimen thickness, transverse strains of polymer B largely decrease near the edges of the analysed surface and reach around  $-0.16$ .

### Strain anisotropy

Due to the large transverse strain gradient measured for polymer B, the analysed surfaces are no longer enough to characterize the global deformation behaviour of the samples. Indeed, the displacement field measurements are performed on 1.8mm of the 3mm thick specimens. The global transverse strains have thus been calculated with Eq. 1 and Eq. 2 from the entire specimen width and thickness measured in pixels on the recorded pictures. The width and the thickness of the specimens have been measured at three different positions along the gauge length on the pictures in order to get an average strain of the entire specimen.

$$\epsilon_{yy}^{av}, images = \ln\left(\frac{w}{w_0}\right) \quad (\text{Eq. 1})$$

$$\epsilon_{zz}^{av}, images = \ln\left(\frac{t}{t_0}\right) \quad (\text{Eq. 2})$$

In Eq. 1 and Eq. 2,  $w$  and  $t$  are respectively the width and the thickness of the specimen from edge to edge and  $w_0$  and  $t_0$  are respectively the width and the thickness measured on the reference image, i.e. the image of the undeformed sample.

The Fig. 9 and Fig. 10 show for both polymers the evolution of the transverse strains  $\epsilon_{yy}^{av}$  and  $\epsilon_{zz}^{av}$  measured with both methods versus the axial strain  $\epsilon_{xx}^{av}$ . For both polymers, the transverse strain  $\epsilon_{yy}^{av}$  decreases almost linearly and a good agreement can be noticed between the two measurement methods. Indeed, in this direction, the analysis is realized on 94% of the specimen width and the error on the global strain is then limited.

On the other hand, through thickness, Fig 9 and Fig 10 show that the measurement method has induced a large

error on the transverse strain  $\epsilon_{zz}^{av}$ . While DIC suggests a stabilization of the average transverse strain, i.e. the stabilization of thickness reduction, the values measured on the images show that the thickness contraction is continuous and that  $\epsilon_{zz}^{av}$  is always larger than  $\epsilon_{yy}^{av}$  until  $\epsilon_{xx}^{av}=49\%$ .

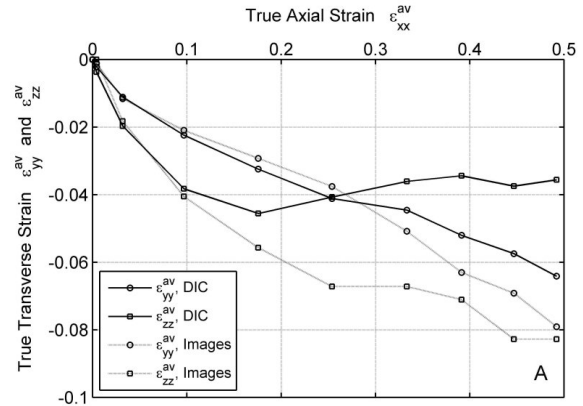


**Fig. 9** – Evolutions of transverse strains measured with both methods versus axial strain for polymer A.

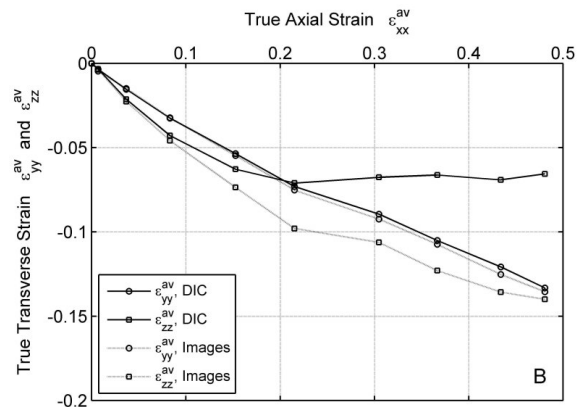


**Fig. 10** – Evolutions of transverse strains measured with both methods versus axial strain for polymer B.

The difference between the measurement results obtained with both methods can be explained by the difference of the analysed thickness on the sample surface. Digital image correlation gives a local information of the deformation behaviour but, as shown in the Fig. 9 and Fig. 10, the studied zone is too small to be representative of the global transverse strain behaviour of the tensile specimen. For all that, both results are complementary and not contradictory.

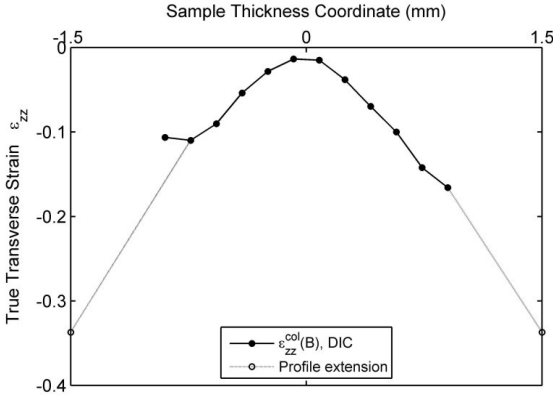


**Fig. 11** – Transverse strain gradient measurements by DIC and direct method for polymer B measured for  $\epsilon_{xx}^{av} = 49\%$ .

The concordance of both methods can be checked by estimating the transverse strain profile over the DIC studied zone. As shown in Fig. 11 for polymer B, this estimation consists in adding two points to the transverse strain gradient  $\epsilon_{zz}^{av}$  on the specimen edges in such a way to find back the thickness variation measured directly on the images. The results show that these two points are in the continuity of the DIC transverse strain profile and so, they confirm the truthfulness of the results. Above all they suggest that the measured strain gradient occurs over the entire specimen thickness.

#### Macroscopic stress-strain behaviour

The macroscopic true axial stress – true axial strain behaviour of the polymers A and B has been determined by calculating the true stress with the Eq. 3 and Eq. 4. In these equations,  $\epsilon_{xx}^{av}$  is the average axial nominal strain, and  $\epsilon_{yy}^{av}$  and  $\epsilon_{zz}^{av}$  are the average transverse nominal strains. The results are plotted in Fig. 12 for polymer A and in Fig. 13 for polymer B.

The true stress has first been calculated with Eq. 3, by using the transverse strains measured by digital image correlation (Fig. 12 and Fig. 13, DIC). It has also been calculated by using the strains determined from the specimen width and thickness on the recorded pictures (Fig. 12 and Fig. 13, images).

$$\sigma_{xx} = \frac{F}{w_0 \times t_0} \times \frac{1}{\left(1 + \epsilon_{yy}^{av}\right) \left(1 + \epsilon_{zz}^{av}\right)} \quad (\text{Eq. 3})$$

$$\sigma_{xx} = \frac{F}{w \times t} \approx \frac{F}{w_0 \times t_0} \times \left(1 + \epsilon_{xx}^{av}\right) \quad (\text{Eq. 4})$$

As shown in Fig. 12 and Fig. 13, the measurement width and thickness has poor influence on the true stress – true strain behaviour. Indeed, even if the large transverse strain gradients induce a large error on the average transverse strain evolutions, the strain intensity is small and the influence on the stress level is then poor.

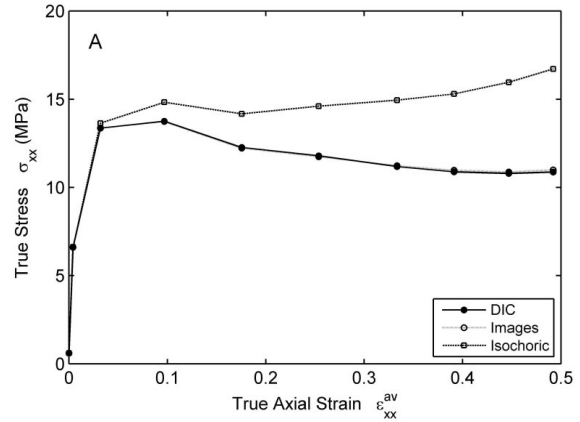


**Fig. 12** – Stress-strain behaviour of polymer A.

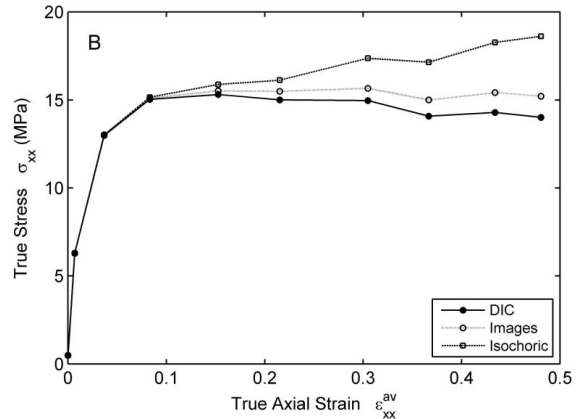


**Fig. 13** – Stress-strain behaviour of polymer B.

When the axial stress is calculated with Eq. 4, the deformation is assumed to be isochoric. As shown in Fig. 12 and Fig. 13, this assumption induces a different mechanical response which is observable for both impact-modified polypropylenes.

Although this assumption is frequently used when the strain is only measured with an axial extensometer, it induces a large overestimation of the plastic behaviour in these impact-modified polypropylenes. For a true axial strain of 49%, the error on the true stress is about 5MPa, i.e. about 30%.

Moreover, whereas the stress calculated with Eq. 3 results in a true stress – true strain curve characterized by a maximum stress at the yield point, the isochoric

assumption induces a maximum strength during the strain hardening.

Until 10% of axial strain, the true stress – true strain curve is however the same whatever the stress calculation method. From this point, which can be considered as the limit of the elastic stage, the mechanical behaviour is governed by a non isochoric deformation process.

Furthermore, the comparison of both polymers indicates that polymer A has a higher elastic modulus than polymer B, but a lower yield stress. This result is in agreement with the literature and is the consequence of the talc content in the impact-modified polypropylene A (Pukanszky et al., 1994).

#### Volumetric strain evolution

The volumetric dilatation of the tensile specimen has been calculated with Eq. 5 within  $\varepsilon_{xx}^{av}$ ,  $\varepsilon_{yy}^{av}$  and

$\varepsilon_{zz}^{av}$  are the average nominal strains determined by digital image correlation in the three directions.

$$\frac{\Delta V}{V_0} = \left(1 + \varepsilon_{xx}^{av}\right)\left(1 + \varepsilon_{yy}^{av}\right)\left(1 + \varepsilon_{zz}^{av}\right) - 1 \quad (\text{Eq. 5})$$

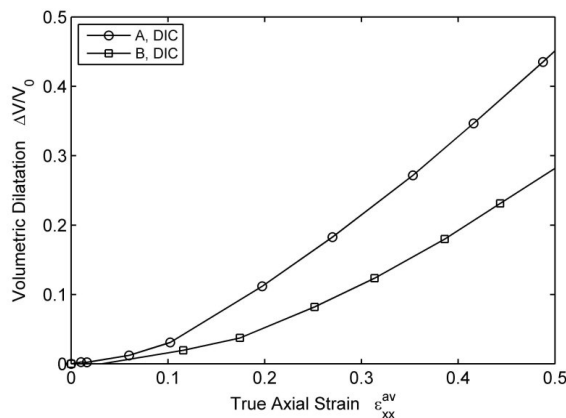


**Fig. 14** – Evolution of the volumetric dilatation of the impact-modified polypropylenes with the average axial strain.

As displayed in Fig. 14, the mechanical behaviour of the impact-modified polypropylenes is characterized by a large volume growth during stretching. After the elastic stage, where a conventional Poisson's effect is observed, an significant dilatation process occurs, leading to a large volumetric dilatation of 45% for polymer A and 28% for polymer B for an average axial strain of 49%.

These volumetric strain results prove that non-cohesive deformation mechanisms and void growth

support a part of the plastic strain and that the plastic deformation is nearly not supported by plastic shearing (G'Sell et al., 2002). Moreover, the faster volumetric dilatation in polymer A indicates that talc has a large influence on the void development, which tallies with the volumetric strain measurements on calcium carbonate high-density polyethylene mentioned by Parsons et al. (2004, 2005).

#### Volumetric dilatation gradients

The macroscopic tensile behaviour has been analysed until now by using the average strains and the spatial resolution of the measurement method has not yet been used to characterize the local deformation of the material. The global approach has however revealed that a too small studied surface can be unsuitable to describe the global deformation behaviour.

Thus, in this study, because of the large transverse strain gradients measured through specimen thickness, a local volumetric analysis has been performed on the materials. As described in Fig. 15, the front and lateral correlation meshes (a), for which strain measurements have been performed for each node, have been projected into the specimen gauge volume respectively along z- and y-axes (b). The intersection of the projected surfaces results in a three-dimensional mesh which correspond to the core part of the specimen gauge volume (c). The dimensions of the obtained fictive specimen volume are  $9.4 \times 9.6 \times 1.8 \text{ mm}^3$ .

As a result of the projection, each node of the 3D mesh includes the information of local strains in all three directions. The local volumetric dilatation can thus be calculated for each three-dimensional mesh node within the fictive volume. Eq. 5 has been used to calculate the local volumetric dilatation at each node by replacing the average nominal strains with the nominal strains.

However, the projection of experimental data is done assuming that the in-plane strain fields measured on the specimen surfaces are representative of the specimen core behaviour and such an assumption can distort the result interpretations in presence of inside strain gradients. Nevertheless, observations of the deformed cross-sections at different strain levels for both composites show that the specimen cross-section remains rectangular during the deformation. Therefore, such strain gradients within the polymers are unlikely and this result reinforce the validity of the previous hypothesis.

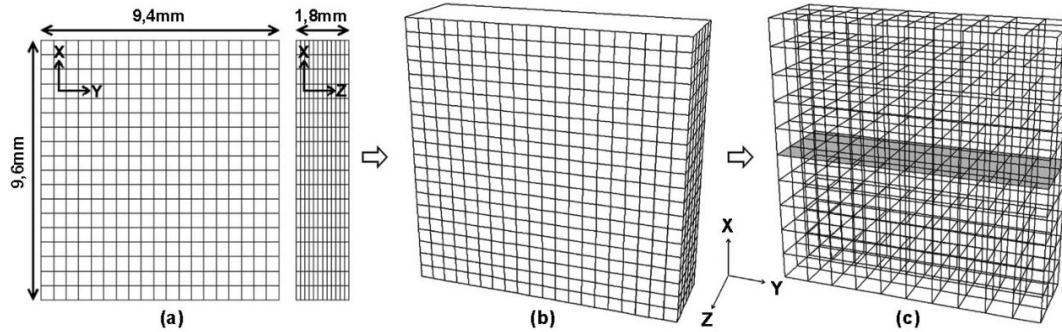


**Fig. 15** – Schematic representation of the experimental data extrapolation to reconstruct the specimen volume.

The local experimental volumetric dilatation values in the central cross-section of the specimen are plotted in Fig. 16 and Fig. 17 for polymer A and B at different loading levels.

One can see in Figs. 10 and 11 that the volumetric dilatation exhibits large gradients within the cross-section which increase like the transverse strain gradient  $\epsilon_{zz}$ .

In composite B, filled with only 0,5% of talc, the large transverse strain gradients observed on both surfaces lead to a volumetric dilatation mainly concentrated along a thickness middle line. For an average axial strain of 52%, the specimen centre shows a volumetric dilatation of about 43%. Near specimen edges, the transverse strains compensate part of the axial strain and, as a result, the local volumetric dilatation is reduced to only 14%.

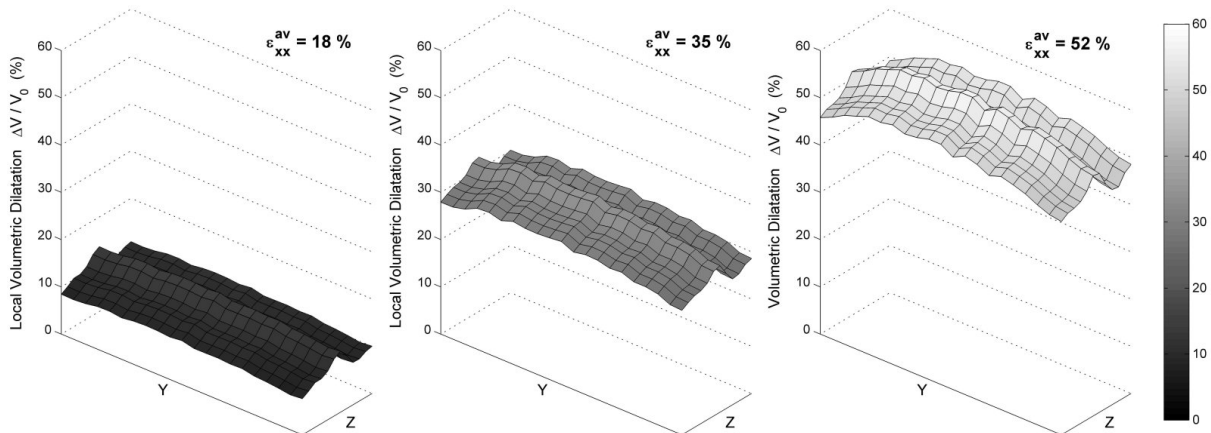


**Fig. 16** - Evolution of experimental volumetric dilatation extrapolated by projection in the specimen cross-section for polymer A.

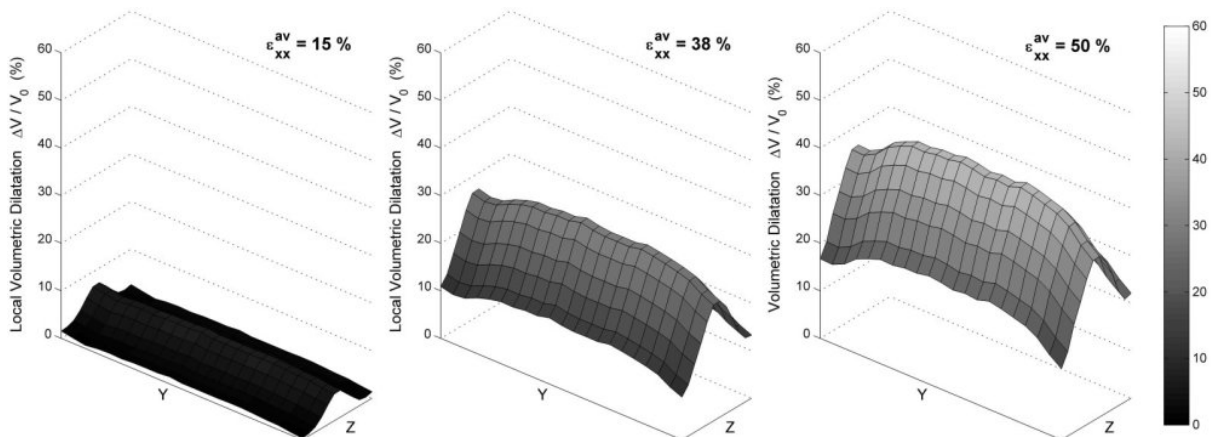


**Fig. 17** - Evolution of experimental volumetric dilatation extrapolated by projection in the specimen cross-section for polymer B.

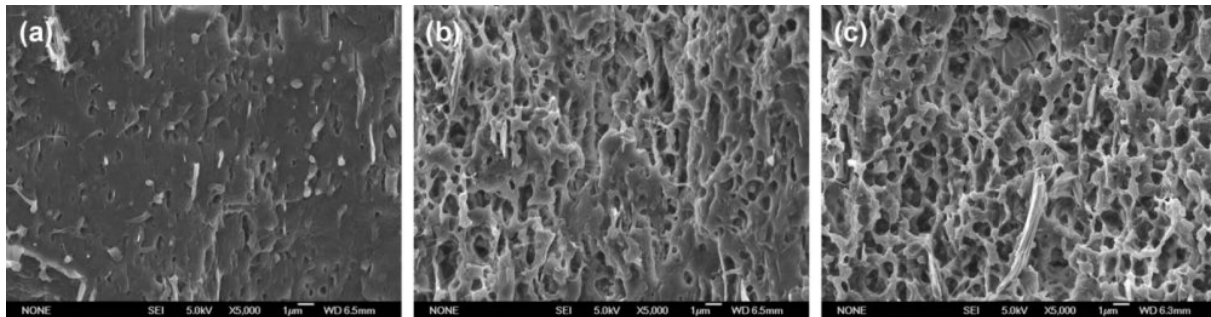


**Fig. 18** – Observation of the deformed microstructure in polymer A for  $\varepsilon_{xx}^{av}=23\%$  ; (a) under the front surface, (c) in the centre of the specimen thickness, (b) at mid-distance of both other pictures.

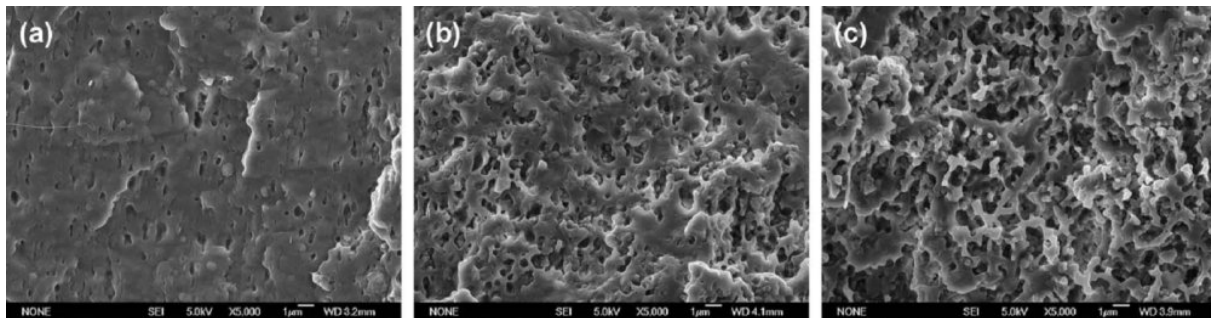


**Fig. 19** - Observation of the deformed microstructure in polymer B for  $\varepsilon_{xx}^{av}=23\%$  ; (a) under the front surface, (c) in the centre of the specimen thickness, (b) at mid-distance of both other pictures.

The local volumetric dilatation gradients in composite A, which contains 4% of talc, are lower than in composite B. The thickness middle line still presents a higher volumetric dilatation level but volumetric dilatation is roughly constant in the entire specimen cross-section. For an average axial strain of 52%, the volumetric dilatation values vary from 55% to 38% from the specimen centre to the edges.

If the evidence of void growth was revealed with the measure of the average volumetric dilatation, the analysis of the local volumetric dilatation through specimen cross-section gives additional information about the distribution of this phenomenon.

#### *Comparison with the deformed microstructure*

As a complement of volumetric dilatation measurements, the deformed microstructures have been investigated by FEG microscopy. The observed surfaces have been obtained by cryogenic fracture performed on specimens previously deformed to an average axial strain of 23% (Fig. 18 and Fig. 19). For both polymers, pictures of the deformed microstructure have been taken under the front surface (a), in the centre of the specimen thickness (c), and at mid-distance of both pictures (b).

The pictures (b) and (c) illustrate the deformed microstructure at mesh nodes for which local

volumetric dilatation has been determined after strain field projection.

The deformed microstructures through specimen thickness, displayed in Fig. 18 for polymer A and in Fig. 19 for polymer B, confirm the existence of volumetric dilatation gradients through thickness. In polymer A (Fig. 18), the pictures (b) and (c) show an advanced void expansion process within specimen cross-section leading to a foam microstructure. In polymer B, this process is delayed in comparison with polymer A, and the dilatation gradient through thickness is obvious. However, in both polymers, the amount of cavities is limited close to specimen front surface (a), on a depth lower than 100µm. According to Stegge and Urban (2001) and Pennington et al. (1999), this depth is the place of surface stratification processes in thermoplastic olefins, which could explain such particular deformed microstructure.

#### *Discussion*

The development of volumetric dilatation in impact-modified-polypropylenes was expected since many authors previously observed the initiation of different kinds of voids in such materials at microscopic scale. In particular, the micromechanical deformation processes of toughened and particle-filled semicrystalline polymers have been well described by Kim and Michler (1998). They have shown that void

formation is caused by either cavitation in the stretched rubbery particles or debonding at the interface between particles and matrix.

Cavitation occurs when the phase adhesion between the modifier and the matrix is good. The plastic deformation then occurs via a cavitation process inside the particles. As shown by Fond et al. (2002), cavitation is a damage mechanism energetically favorable when the applied tension induces large hydrostatic stress to a particle.

Under the effect of hydrostatic stress, debonding can be an important damage mechanism when the adhesion between the different phases is poor. It is consistently observed around rigid particles and it can lead to a considerable damage rate (G'sell et al., 2004).

In the present studied impact-modified polypropylenes, the void initiation could not be identified, but the different nature of the particles suggest that both damage mechanisms are active.

Apart from the nature of the fillers, the higher particle content in polymer A can explain a part of the high damage rate in this material. Nevertheless, talc debonding has been observed in both materials on cryogenic fracture surface of the deformed samples and this mechanism is probably partly responsible for the high damage rate of polymer A upon stretching.

But if the composition of the polymers can explain the global volumetric behaviour of both impact-modified polypropylenes, they are not sufficient to clarify the existence of the cavity gradients through specimen cross section as revealed by FEG investigation and volumetric dilatation measurements.

Indeed, these gradients may be induced either by scale/edge effects, i.e. geometrical consideration, or by the moulding process conditions and in particular by the cooling rate gradients through specimen thickness. The specimen were machined from 3mm thick injected plates and so the microstructure can be considered as homogeneous along the specimen width. Moreover, strain gradients are small and are only visible for a few millimetres on both sides of the centre part of the specimen. As a result, the volumetric gradients in this direction may be the consequence of the specimen geometry.

Through thickness, the larger volumetric dilatation has been measured along a centre line in both materials which remind the optical heterogeneity already mentioned when presenting the materials. In material B, the larger dilatation gradient matches with the wider optical heterogeneity and on the contrary, the polymer A exhibits a narrow heterogeneity within specimen thickness.

The results of the present investigation then suggest that this white centre line is actually the sign of damage inside the unloaded material, as a consequence of the

moulding process. This damage would be induced by the accumulation of residual stress in the specimen core during cooling.

Indeed, elastomer has a noticeably lower thermal conductivity than the matrix and as a result, the fillers reduce the cooling rates in specimen core. This effect is however only perceptible in specimen core because the difference of thermal conductivity does not affect the polymer that is in contact with the mould which is quenched immediately.

Talc particles exhibit a higher thermal conductivity than the matrix (Droval et al., 2005). Thus, in polymer A, the cooling rate of the specimen core could be enhanced and the white centre line width be reduced.

Thus, when the polymer is deformed, the void extension process would be accelerated by this inside pre-damage and would lead to cavity gradients through specimen thickness.

## Conclusions

The plastic deformation of two impact-modified polypropylenes have been studied experimentally by using a novel measurement technique based on digital image correlation. The set-up and the measurement procedures have been developed in order to measure the local strains in the three directions on the surface of tensile test specimens with good accuracy. By using the strain fields, the mechanical response of the materials can be determined without using any isotropic assumption.

Both impact-modified polypropylenes mainly differ in their talc content (4% in A while it is only 0.5% in B). The influence of talc can be noticed on the mechanical response (modulus, yield strength) and on the volumetric dilatation. The true stress – true strain behaviour, as well as the volumetric dilatation could be identified and have confirmed the non isochoric plastic deformation of both materials due to void extension during the tension tests.

But above all, the local strains have revealed the existence of transvers strain gradients that have an incidence on the mechanical behaviour of the materials. In polymer B, the transverse strain gradients induce large dilatation gradients through specimen cross-section while in polymer A, the deformation is roughly homogeneous. The presence of such gradients can be explained by the difference of thermal conductivity of the different phases inside the material and their influence on the local cooling rates.

## Acknowledgements

The authors would like to thank the ADEME (Agence pour le Développement de l'Environnement et de la Maîtrise des Energies), the Région Poitou-Charentes

and Research Ministry - through ACI Recypro B - for sponsoring this work.

## References

Brillaud J, Lagattu-Touchard F., "Limits and possibilities of laser speckle and white light image correlation methods: theory and experiments", *Applied Optics*, 41, 6603-6613 (2002)

De Almeida O., Lagattu F., Brillaud J., "Analysis by a 3D DIC of volumetric deformation gradients: Application to polypropylene/EPR/talc composites", *Comp. Part A : Applied Sci. and Manufacturing*, 39, 1210-1217 (2008)

Delaval D., Casetta M., Delobel R., Traisnel M., Guillet J., Raveyre C., Bourbigot S., "Thermal and fire degradation of recycled and polluted polypropylene-based materials", *J. Applied Pol. Sci.*, 112, 2270-2279 (2009)

Droval G., Glouannec P., Feller J.F., Salagnac P., "Simulation of electrical and thermal behavior of diphasic conductive polymer composites heating elements", *J Thermophys Heat Transf*, 19, 375-381 (2005)

Fond C., Géhant S., Schirrer R., "Effects of mechanical interactions on the hydrostatic stress in randomly distributed rubber particles in an amorphous polymer matrix", *Polymer*, 43, 909-919 (2002)

G'Sell C., Hiver J.M., Dahoun A., "Experimental characterization of deformation damage in solid polymers under tension, and its interrelation with necking", *Int. J. of Sol. and Struct.*, 39, 3857-3872 (2002)

G'Sell C., Bai S.-L., Hiver J.-M., "Polypropylene/polyamide 6/polyethylene-octene elastomer blends. Part 2: volume dilatation during plastic deformation under uniaxial tension", *Polymer*, 45, 5785-5792 (2004)

Kim G.-M. and Michler G. H., "Micromechanical deformation processes in toughened and particle-filled semicrystalline polymers: Part 1. Characterization of deformation processes in dependence on phase morphology", *Polymer*, 39, 5689-5697 (1998)

Parsons E., Boyce M.C., Parks D.M., "An experimental investigation of the large-strain tensile behavior of neat and rubber-toughened polycarbonate", *Polymer*, 45, 2665-2684, (2004)

Parsons E.M., Boyce M.C., Parks D.M., Weinberg M., "Three-dimensional large-strain tensile deformation of neat and calcium carbonate-filled high-density polyethylene", *Polymer*, 46, 2257-2265 (2005)

Pennington B.D., Rytz R.A., Urban M.W., "Stratification in thermoplastic olefins (TPO); photoacoustic FT-IR depth profiling studies", *Polymer*, 40, 4795-4803 (1999)

Pukánszky B, Belina K., Rockenbauer A., Maurer F.H.J., "Effect of nucleation, filler anisotropy and orientation on the properties of PP composites", *Composites*, 25, 205-214 (1994)

Stegge J. M., Urban M. W., "Stratification processes in thermoplastic olefins monitored by step-scan photoacoustic FT-IR spectroscopy", 42, 5479-5484 (2001)

Viana J.C., "Development of the skin layer in injection moulding: phenomenological model", *Polymer*, 45, 993-1005 (2004)